MINISTÉRIO DA CIÊNCIA E TECNOLOGIA
INSTITUTO NACIONAL DE PESQUISAS ESPACIAIS

IUGG-1803

IAGA

26th IUGG GENERAL ASSEMBLY
PRAGUE 2015

Solar Activity Dependence of the E-Region Electric Field in the Brazilian Equatorial Sector

C. M. Denardini[1], S. S. Chen[1,2], J. Moro[1] ,
L. C. A. Resende[1], N. J. Schuch[3], J. E. R. Costa[1]

[1] National Institute for Space Research (INPE), S. J. Campos-SP, Brazil
[2] Universidade de Taubaté (UNITAU), Taubaté-SP, Brazil
[3] Southern Regional Space Research Center (INPE), Santa Maria, RS, Brazil

A43 Charact. Ionosph. and Magnet. Processe from Ground and Satellite Observ. and their Connection to Space Weather (ICDC/Div. II/Div. III/Div. V) – Wednesday Jul 24 09:45 LT - South Hall 2

Introduction

- The day-to-day variabilities of the EEJ under auroral activity and quiet conditions -

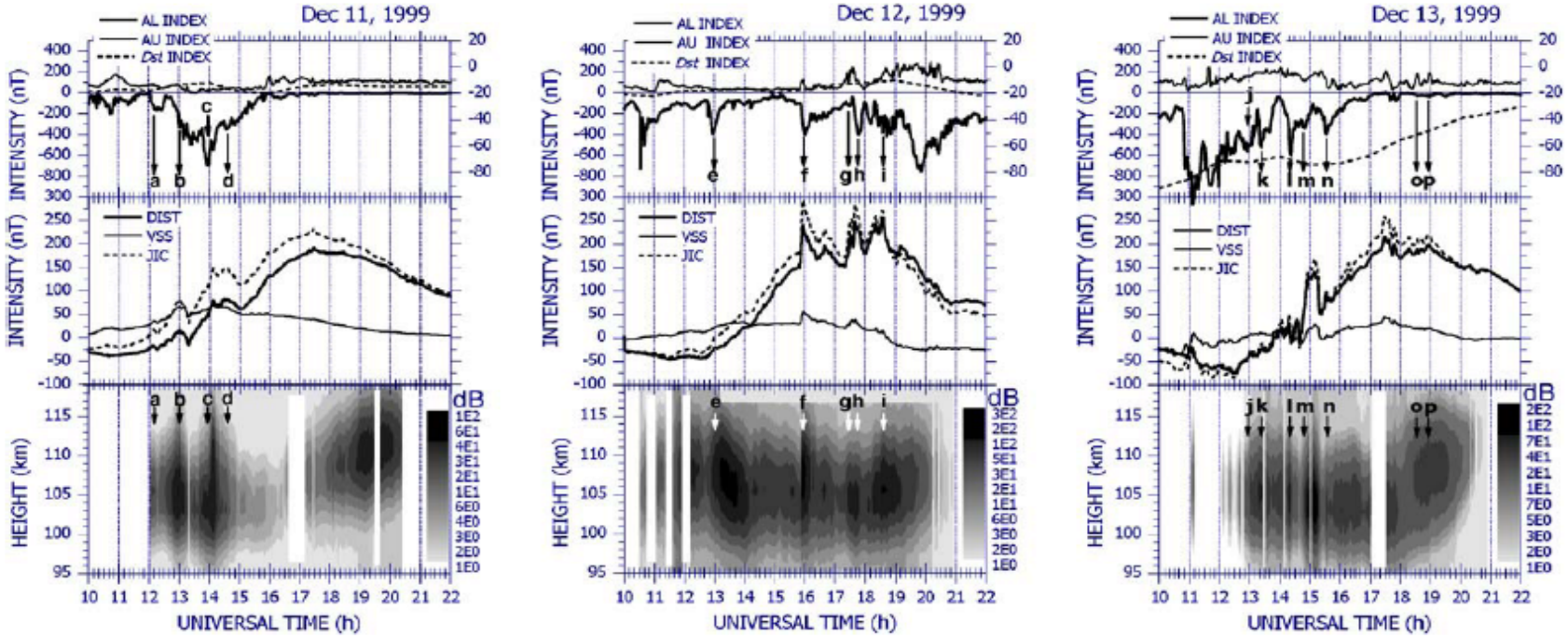

Fig. 2. Range–Time–Intensity (RTI) maps from three disturbed days: December 11th, 12th and 13th, from the RESCO 50 MHz coherent radar (bottom panel). On the top panel of each graph is shown the variation of the auroral indices AU (continuous thin line) and AL (continuous fat line) referred to the left axis scale and the variation of the ring current index D_{st} (dotted line) referred to the right axis scale. The middle panel shows the variation of the horizontal component of the Earth's magnetic field (ΔH) over Vassouras (continuous thin line) and that over Jicamarca (dotted line). The continuous thick line represents the disturbance effect obtained by the difference between the ΔH components over Jicamarca and Vassouras.

AFTER: Denardini, C. M.; Abdu, M. A. ; Sobral, J. H. A. (2004). VHF radar studies of the equatorial electrojet 3-m irregularities over São Luís: day-to-day variabilities under auroral activity and quiet conditions. Journal of Atmospheric and Solar-Terrestrial Physics, 66(17), p.1603-1613.

Introduction

- The seasonal characterizations of the EEJ in the Brazilian sector -

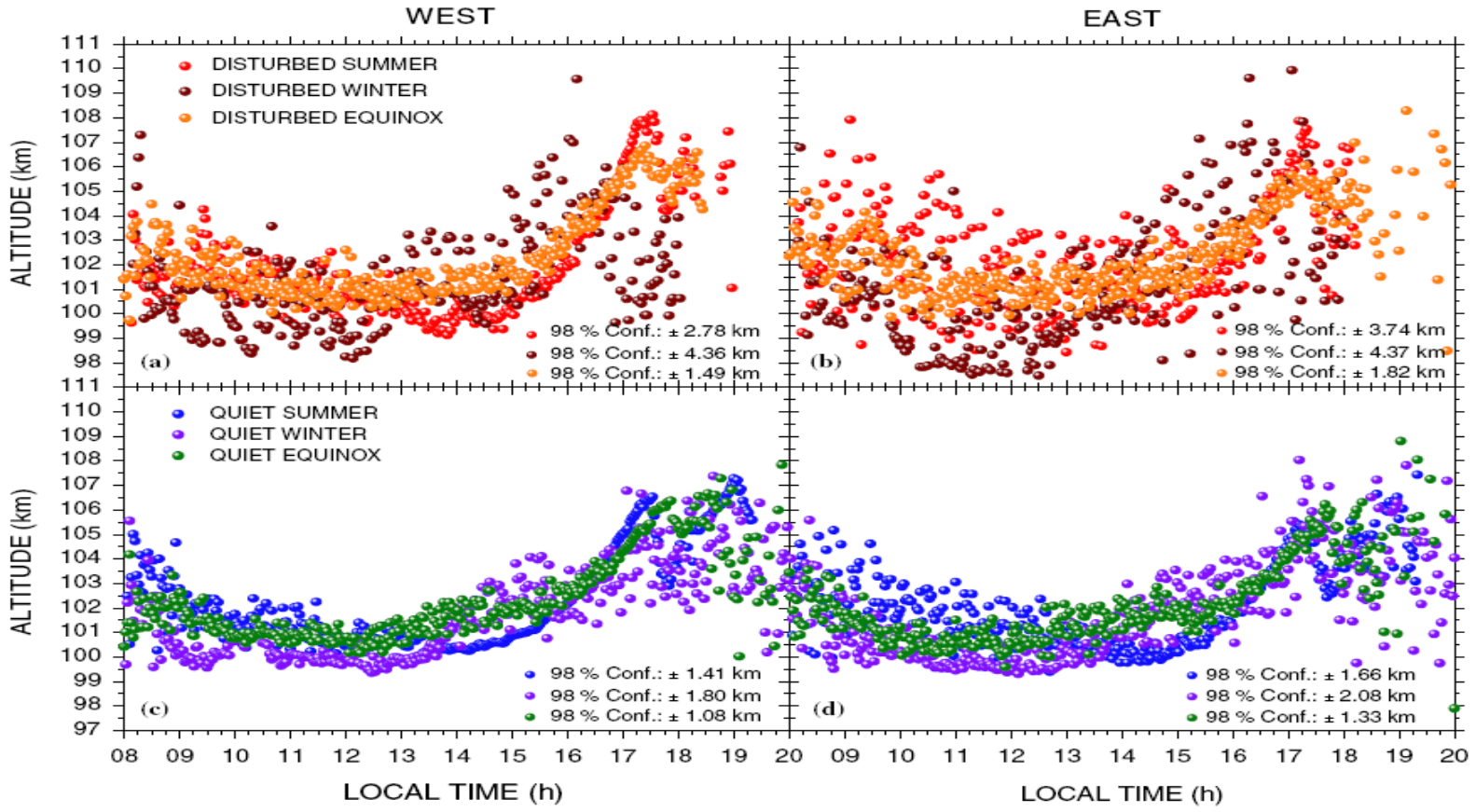

Fig. 2. Diurnal variation of the mean EJC, obtained from disturbed ("a" and "b") and quiet ("a" and "b") periods, separated according the radar beam and season. The daily mean limits of confidence are presented at the right bottom corner in each panel and were calculated for 98% of statistical confidence.

AFTER: Denardini, C. M.; Abdu, M. A.; De Paula, E. R.; Sobral, J. H. A.; Wrasse, C. M. (2005). Seasonal characterization of the equatorial electrojet height rise over Brazil as observed by the RESCO 50MHz back-scatter radar. Journal of Atmospheric and Solar-Terrestrial Physics, 67, p. 1665-1673.

Introduction

- The transition from day to night-time (pre-reversal electrodynamic enhancement) -

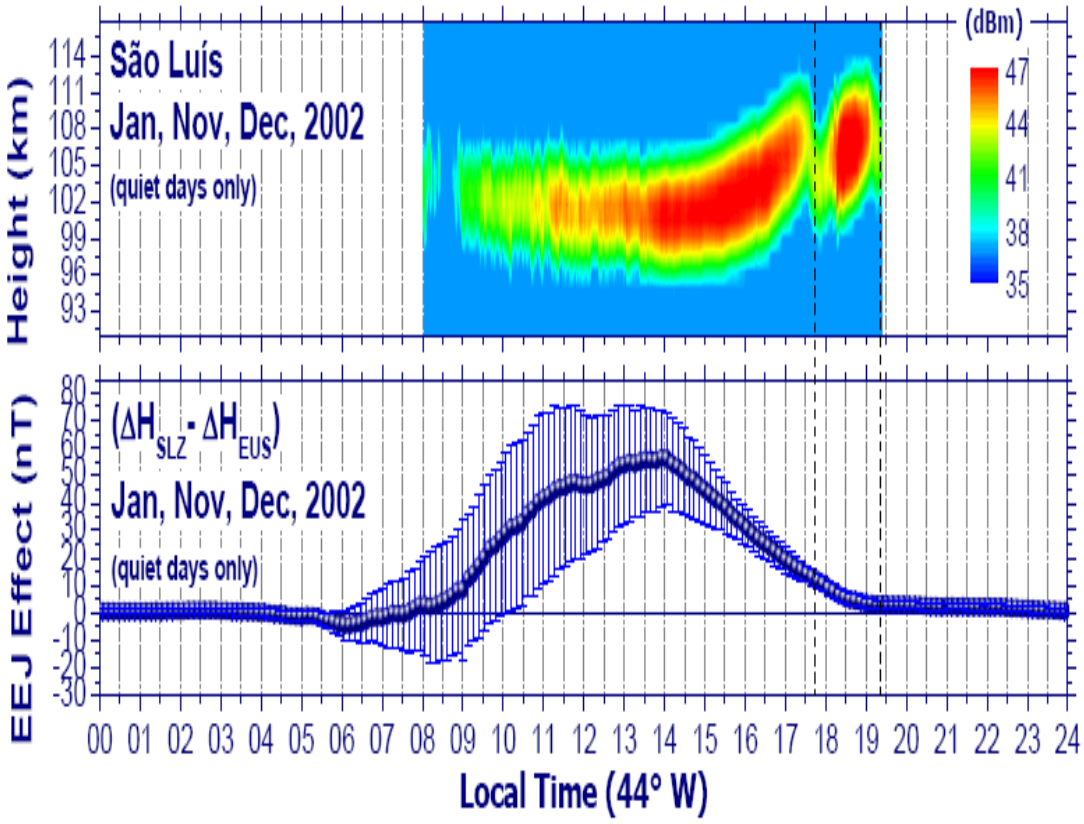

Fig. 1. Upper panel: mean RTI map obtained for the quiet period ($K_p \leq 3+$) using the RESCO radar during the Southern Hemisphere summer solstice. The colour scale gives the signal power. Bottom panel: Mean diurnal variation of the $\Delta H = \Delta H_{SLZ} - \Delta H_{EUS}$ for the same period of upper mean RTI map, representing the EEJ ground effect (strength), deduced from variations of the H component of the Earth's magnetic field measured by magnetometers in São Luís and Eusébio, respectively.

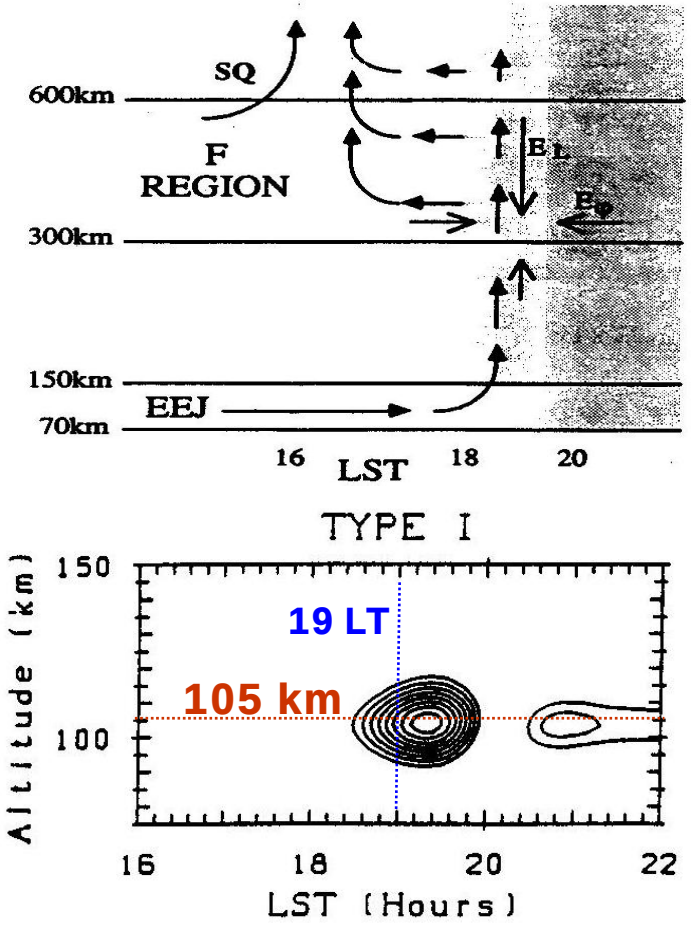

Haerendel and Eccles, **JGR** (1992)

AFTER: Denardini, C. M.; Abdu, M. A.; de Paula, E. R.; Wrasse, C. M.; Sobral, J. H. A. (2006). VHF radar observations of the dip equatorial E-region during sunset in the Brazilian sector. Annales Geophysicae, Toulouse, 24(1-7), p. 1617-1623.

Introduction

- Climatology of GW-induced electric fields in the equatorial E region -

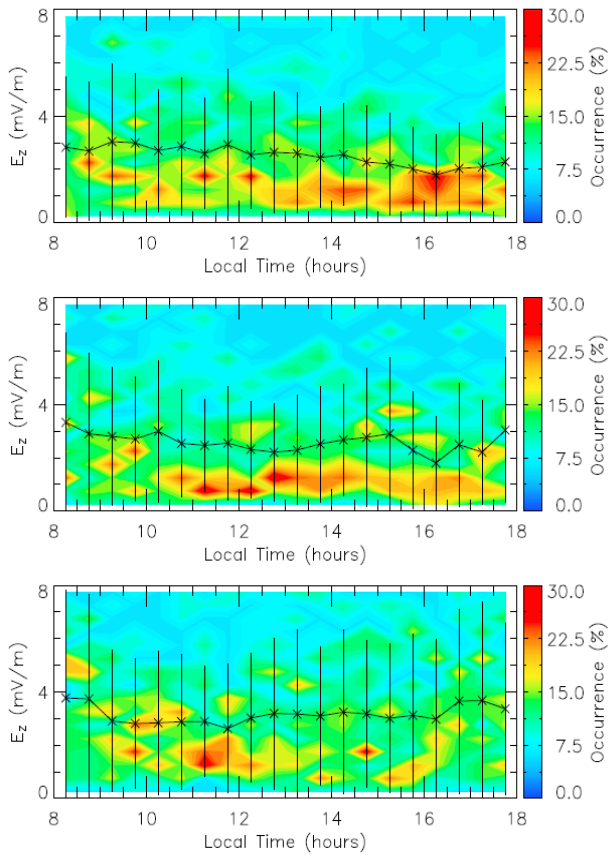

Figure 2. Statistics of occurrences of E_z amplitude as function of time for (top) solstice D months, (middle) equinoctial E months, and (bottom) solstice J months. The continuous line represents the average vertical electric field for each 30-min interval, and the vertical line is the standard deviation of E_z.

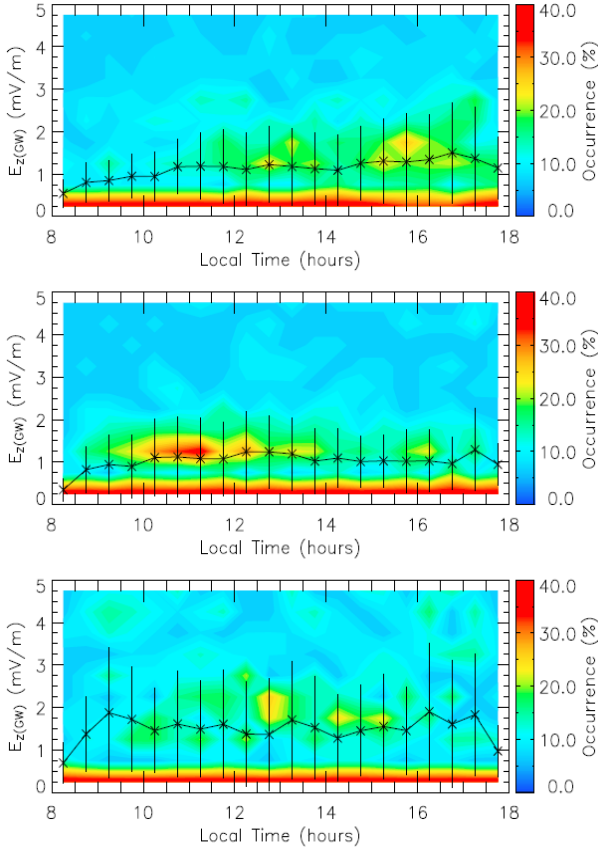

Figure 3. Statistics of occurrences of the $E_{z(GW)}$ amplitude as function of time for (top) solstice D months, (middle) equinoctial E months, and (bottom) solstice J months. The continuous line represents the average disturbed electric field for each 30-min interval, and the vertical line is the standard deviation of $E_{z(GW)}$.

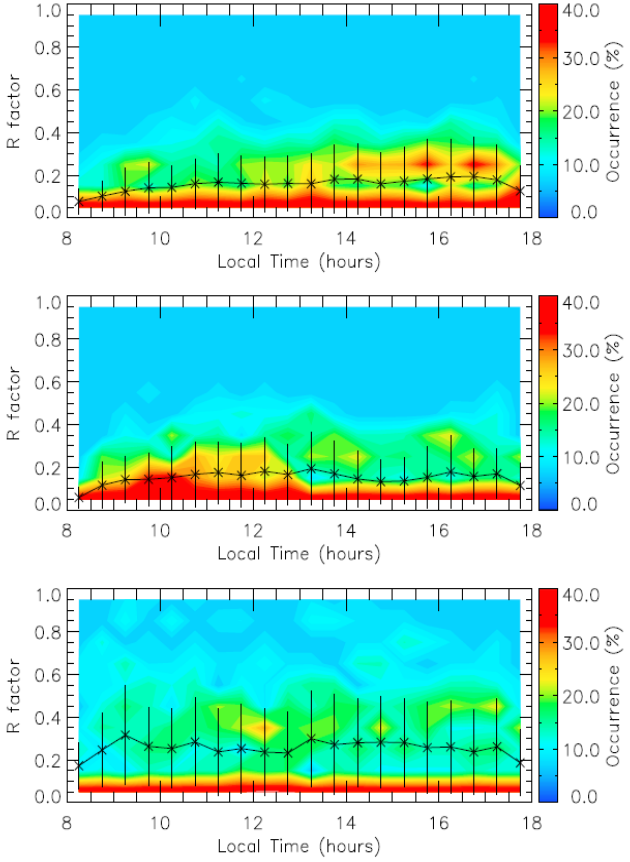

Figure 4. Statistics of occurrences of the R_{GW} as function of time for (top) solstice D months, (middle) equinoctial E months, and (bottom) solstice J months. The continuous line represents the average factor for each 30-min interval, and the vertical line is the standard deviation of R_{GW}.

AFTER: Aveiro, H. C.; Denardini, C.M. ; Abdu, M. A. (2009a). Climatology of gravity waves induced electric fields in the equatorial E region. Journal of Geophysical Research, 114, p. 10.1029/2009JA0.

Introduction

- The anomalous conductivity effects on the EEJ electric fields -

Table 1

Zonal electric field estimated and/or supposed at E region heights for the Peruvian, Indian and Brazilian sectors.

Reference	ZONAL EF (mV/m)	SECTOR
Sugiura and Cain (1966)	2, 4 [mean]	Peruvian
Balsley and Woodman (1971)	~0.38–2.06	Peruvian
Balsley (1973)	~0.1–0.8 [8–18 LT]	Peruvian
Schieldge et al. (1973)	~0.8 [local midday]	Indian
Reddy (1977)	0.3 [assumed value]	Model
Marriott et al. (1979)	1 [typical value]	Model [Peruvian]
Viswanathan et al. (1987)	~0.1–0.6 [8–18 LT]	Indian
Reddy et al. (1987)	~0.1–0.55 [8–18 LT]	Indian
Kelley (1989)	~0.5	Generalized
Viswanathan et al. (1993)	~0.3–0.5 [9–14 LT]	Indian
Present work	0.13–0.49 [8–18 LT]	Brazilian

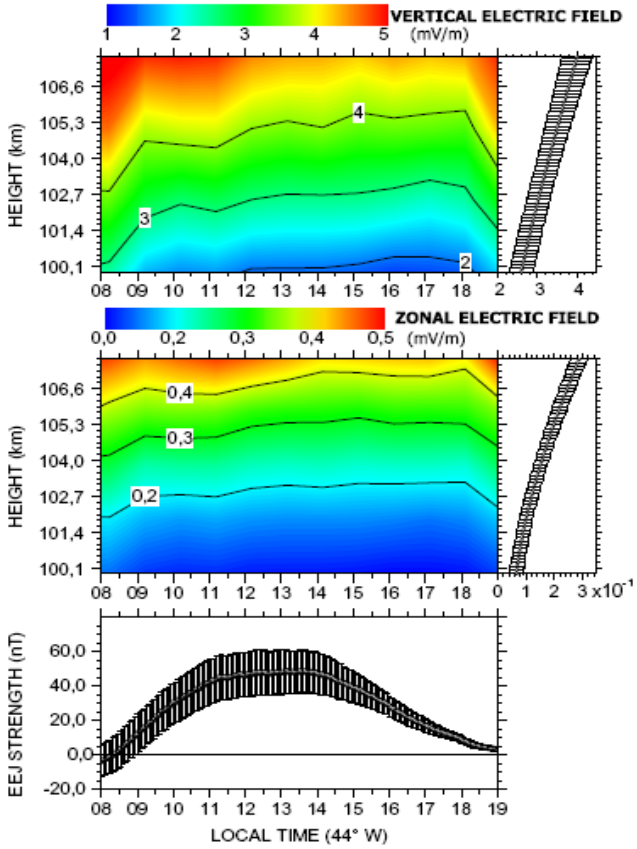

Fig. 2. Mean (upper panel) vertical electric field (E_z) map, mean (middle panel) zonal electric field (E_y) map and mean (lower panel) EEJ ground strength diurnal variation obtained during 63 magnetically quiet day in 2002.

AFTER: Denardini, C.M.; Aveiro, H.C.; Sobral, J.H.A.; Bageston, J.V., L.M. Guizelli, L.C.A. Resende a, J. Moro (2013). E region electric fields at the dip equator and anomalous conductivity effects. Advances in Space Research, 51, p.1857.1869.

Introduction

- The anomalous conductivity effects on the EEJ electric fields -

Appendix A. Set of collision rates equation

In the following we enroll the collision rates equation used for all species considered in our model (Schunk et al., 1996).

Molecular oxygen (O_2^+) – Neutral:

$$\nu_{O_2^+ \to O} = 2.31 \times 10^{-10} \cdot n[O]$$

$$\nu_{O_2^+ \to O_2} = 2.55 \times 10^{-11} \cdot n[O_2] \cdot T^{1/2} \cdot (1 - 0.073 \cdot \log(T))^2 \quad (5)$$

$$\nu_{O_2^+ \to N_2} = 4.13 \times 10^{-10} \cdot n[N_2]$$

Nitric oxide (NO^+) – Neutral:

$$\nu_{NO^+ \to O} = 2.44 \times 10^{-10} \cdot n[O]$$

$$\nu_{NO^+ \to O_2} = 4.27 \times 10^{-10} \cdot n[O_2] \quad (6)$$

$$\nu_{NO^+ \to N_2} = 4.34 \times 10^{-10} \cdot n[N_2]$$

Atomic oxygen (O^+) – Neutral:

$$\nu_{O^+ \to O} = 4.45 \times 10^{-11} \cdot n[O] \cdot T^{1/2} \cdot (1.04 - 0.067 \cdot \log(T))^2$$

$$\nu_{O^+ \to O_2} = 6.64 \times 10^{-10} \cdot n[O_2] \quad (7)$$

$$\nu_{O^+ \to N_2} = 6.82 \times 10^{-10} \cdot n[N_2]$$

Electron – Neutral:

$$\nu_{e \to O} = 8.20 \times 10^{-10} \cdot n[O] \cdot T^{1/2}$$

$$\nu_{e \to O_2} = 1.80 \times 10^{-10} \cdot n[O_2] \cdot T^{1/2} \cdot (1. + 3.6 \times 10^{-2} \cdot T^{1/2}) \quad (8)$$

$$\nu_{e \to N_2} = 2.33 \times 10^{-11} \cdot n[N_2] \cdot T \cdot (1. - 1.2 \times 10^{-4} \cdot T)$$

In this set $n[X]$ is the density of the generic constituent X, T is the electron temperature, which can be approximated to the neutral temperature in the lower E region without significant effect on the conductivities (Denardini, 2007).

The gyrofrequencies were calculated, as per equation:

$$\omega_{e,i} = \frac{q_{e,i} B}{m_{e,i}}, \quad (9)$$

where $m_{e,i}$ is the mass average, and $q_{e,i}$ is the electrical charge. The subscript e and i indicate the electron and ion terms, respectively.

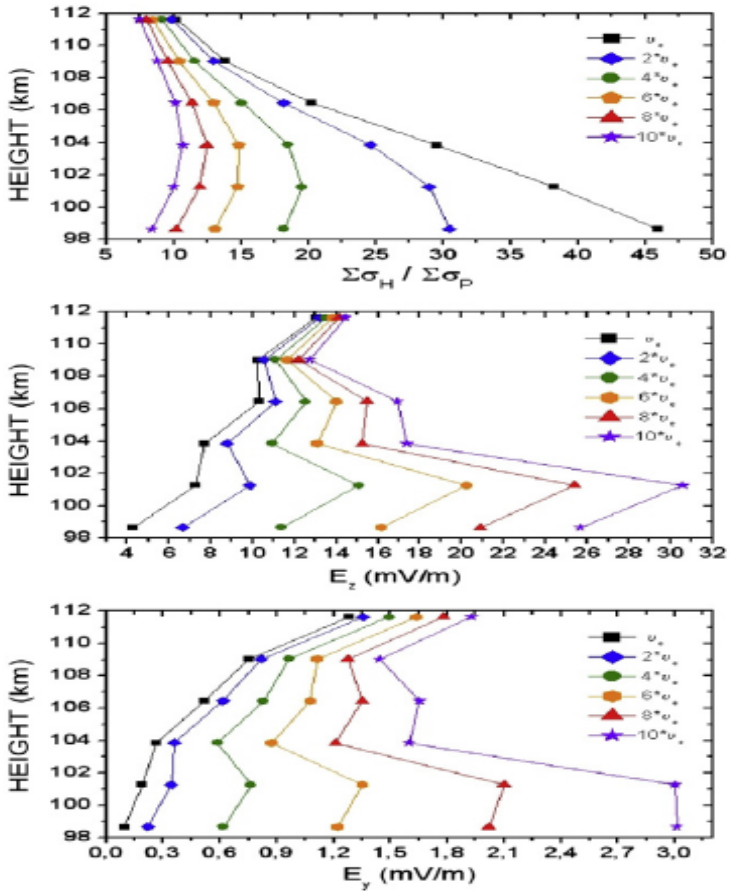

Fig. 8. Vertical profiles of (upper) Hall-to-Pedersen integrated conductivities, (middle) vertical electric field (E_z), and (lower) zonal electric field (E_y) derived from the RESCO radar at 12 LT on January 29, 2002.

AFTER: Denardini, C.M.; Aveiro, H.C.; Sobral, J.H.A.; Bageston, J.V., L.M. Guizelli, L.C.A. Resende a, J. Moro (2013). E region electric fields at the dip equator and anomalous conductivity effects. Advances in Space Research, 51, p.1857.1869.

Methodology

- About the data selection and analysis -

For the present study:

1. we have selected coherent VHF backscatter radar data collected
2. during geomagnetically quiet days ($Kp \leq 3$) only,
3. covering the year from 2001 through 2010,
4. collected in the Brazilian dip equator.
5. We estimate the vertical component of the electric field (Ez) and the zonal component of the electric field (Ey).
6. The diurnal variation of these quantities was then evaluated considering the solar activity during the last solar cycle.

Methodology

- The RESCO radar -

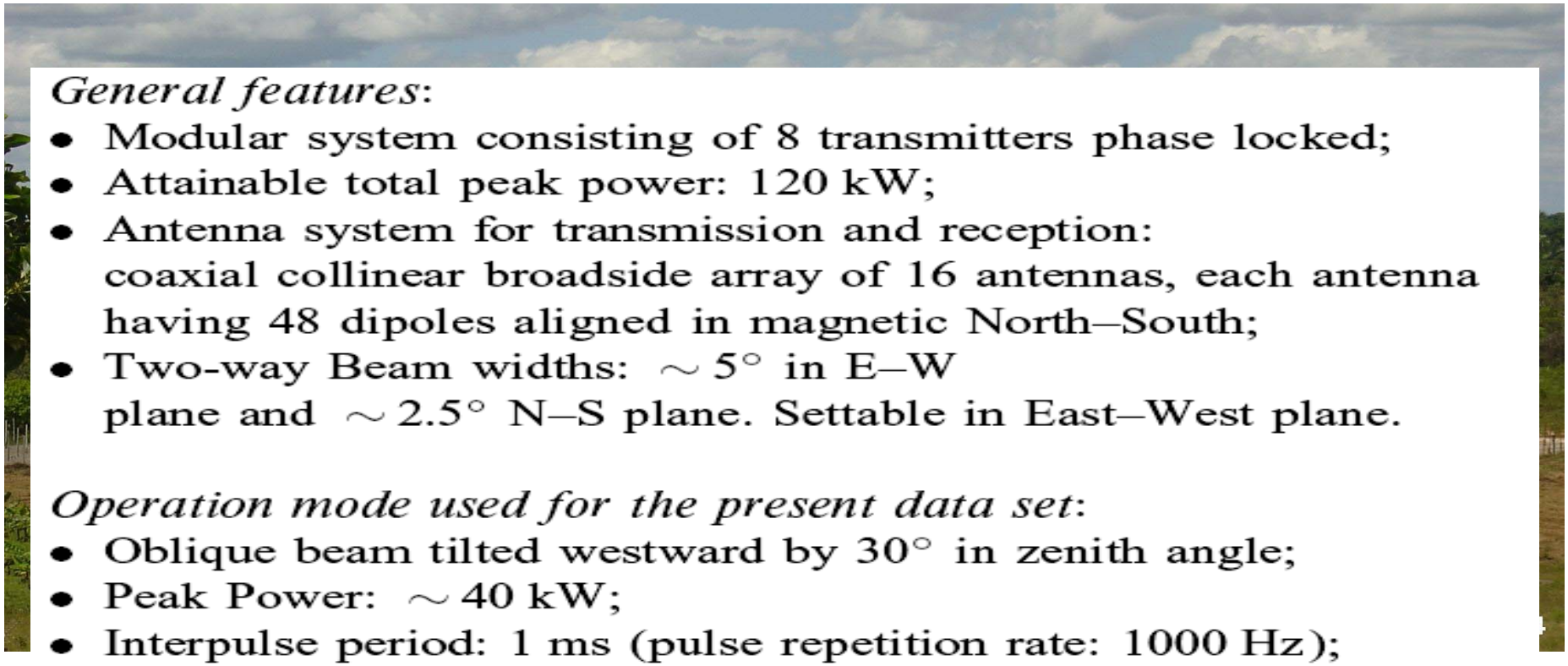

General features:

- Modular system consisting of 8 transmitters phase locked;
- Attainable total peak power: 120 kW;
- Antenna system for transmission and reception: coaxial collinear broadside array of 16 antennas, each antenna having 48 dipoles aligned in magnetic North–South;
- Two-way Beam widths: $\sim 5°$ in E–W plane and $\sim 2.5°$ N–S plane. Settable in East–West plane.

Operation mode used for the present data set:

- Oblique beam tilted westward by 30° in zenith angle;
- Peak Power: ~ 40 kW;
- Interpulse period: 1 ms (pulse repetition rate: 1000 Hz);
- Pulse width: 20 μs;
- Echo sampling: 3 km in range or 2.6 km in height;
- Theoretically estimated height resolution: 7.5 km (for the oblique beam at 30° zenith angle);
- Data rate: one power spectrum (of 512 points) per 6 s.

Methodology

- Power Spectra -

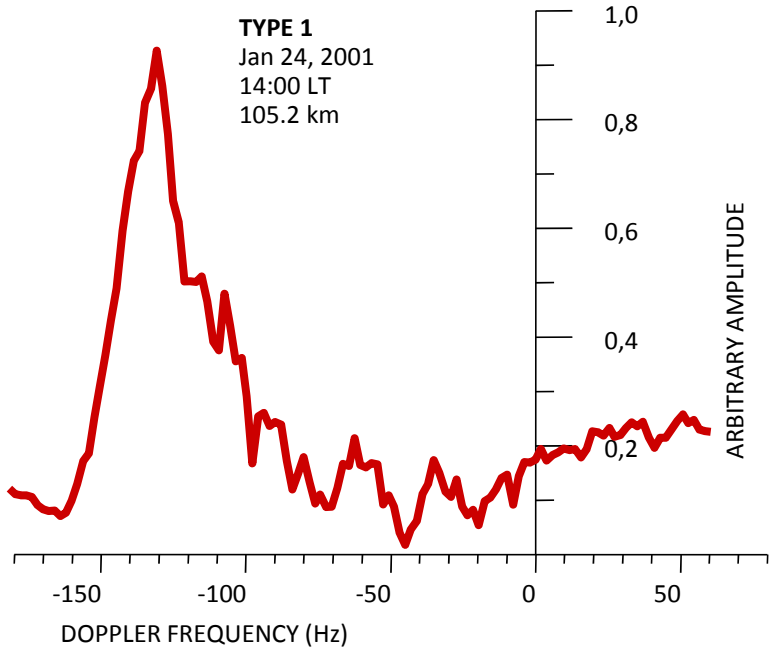

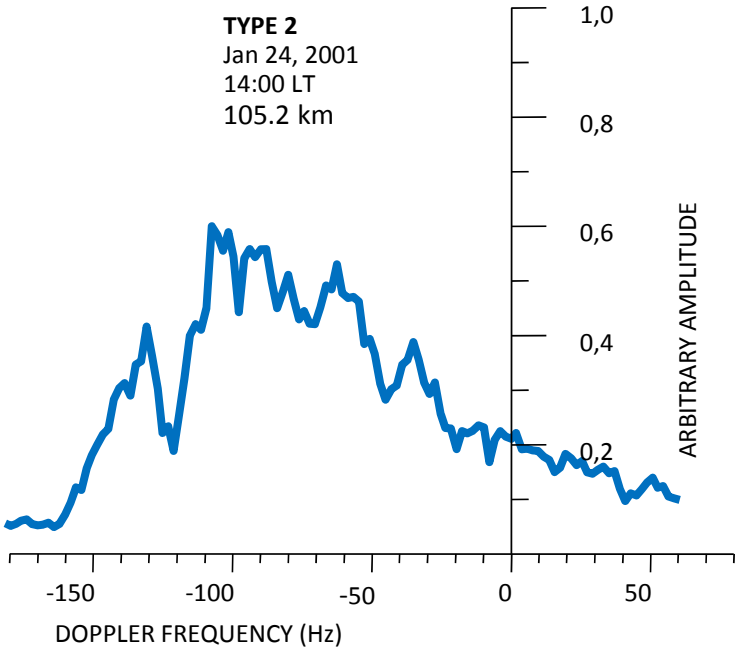

TYPE 1:

- Two-stream instability;
- Velocity close to the ion-acoustic speed (360 m/s);
- Narrower and with higher amplitude spectrum; and
- Observed in the upper part of EEJ scattering region.

TYPE 2:

- Gradient drift instability;
- Velocity proportional to $E \times B/B^2$;
- Broader and with smaller amplitude spectrum; and
- Observed in the lower part of EEJ scattering region.

Methodology

- The basic processing -

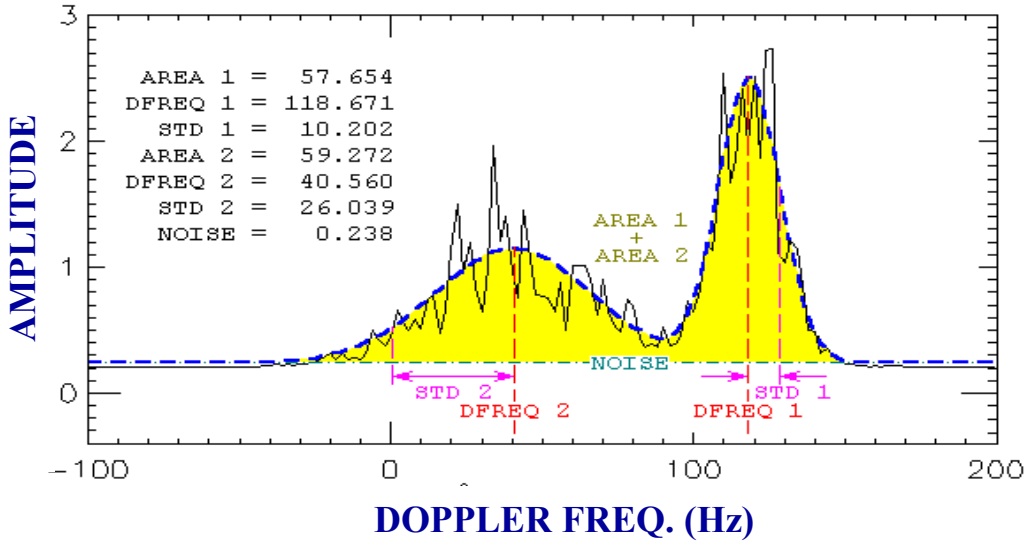

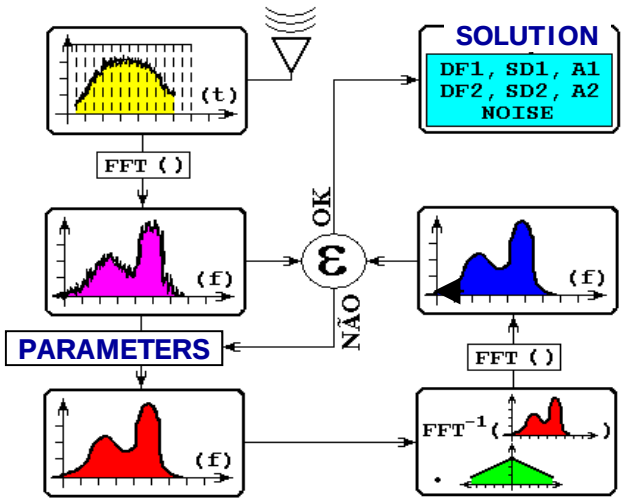

Two Gaussian curves are fitted to each spectrum, as given by:

$$S(f) = \frac{P_1}{\sigma_1\sqrt{2\pi}}\exp\left[-\frac{(f-f_{D1})^2}{2\sigma_1}\right] + \frac{P_2}{\sigma_2\sqrt{2\pi}}\exp\left[-\frac{(f-f_{D2})^2}{2\sigma_2}\right] + P_N$$

Type 1 Type 2 Noise

Methodology

- The electric field computing -

$$\vec{V} = \frac{\vec{E} \times \vec{B}}{\left|\vec{B}\right|^2}$$

Type 2 velocity

Geomagnetic field

$$E_z = \frac{1}{1+\psi} \frac{V_{D2} \cdot B^2}{H}$$

Anisotropic factor

H-component of **B**

$$\psi = \frac{\nu_e \cdot \nu_i}{\Omega_e \cdot \Omega_i}$$

Parameters obtained by atmospheric models

$$E_o = \frac{\int_{-\theta}^{+\theta} \sigma_P \cdot r \cdot d\theta}{\int_{-\theta}^{+\theta} \sigma_H \cdot r \cdot d\theta} \cdot E_z \Rightarrow E_o = \frac{\Sigma_P}{\Sigma_H} \cdot E_z.$$

Methodology

- The F10.7 solar flux from 2001 to 2010 -

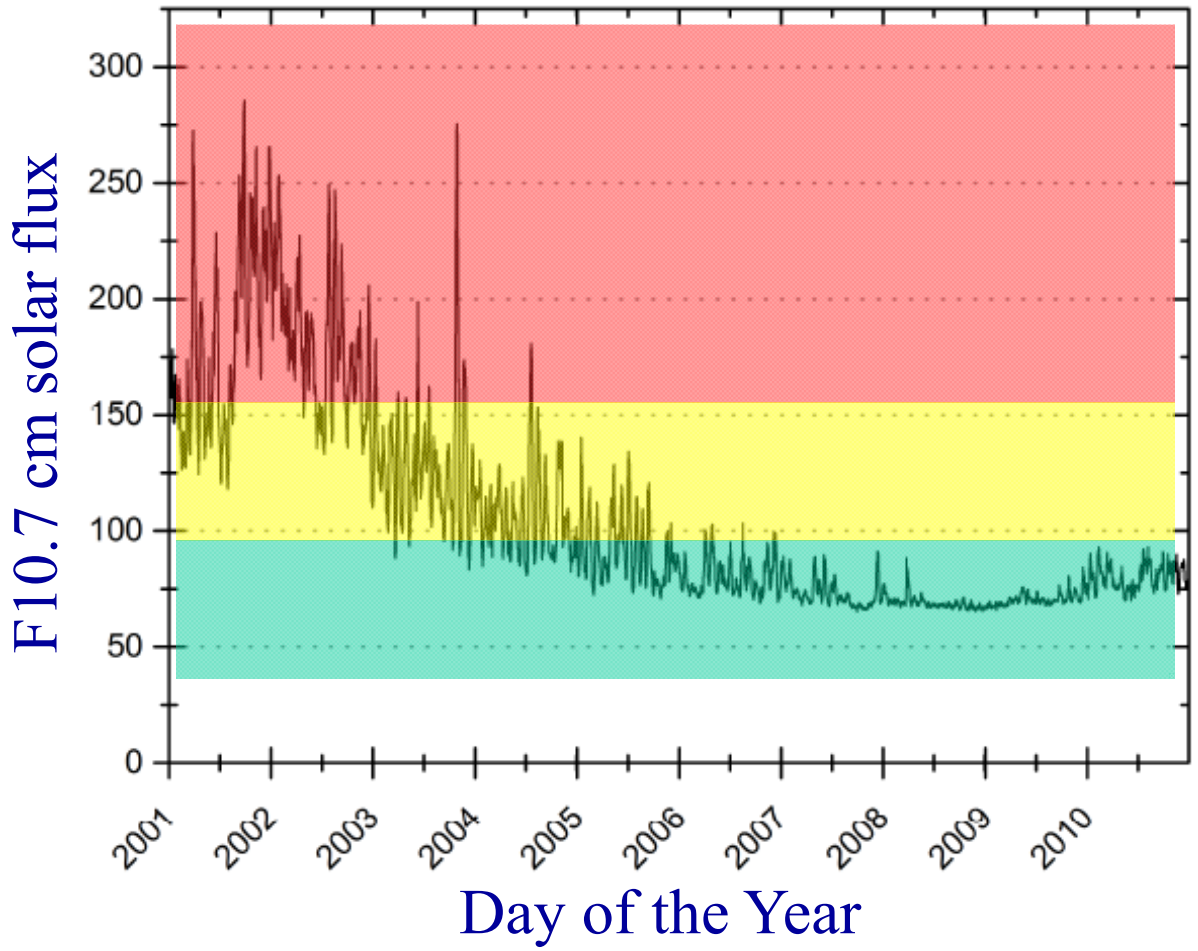

We have used the F10.7 solar flux [10^{-22} W m^{-2} Hz^{-1}] which is the electromagnetic solar emission at λ = 10.7 cm (2.8 GHz).

The daily averaged F10.7 is a solar index, and provides a proxy to the solar ultraviolet radiation flux, responsible for most of the photoionization of the ionosphere.

In the period of high solar activity (2001-2002) the F10.7 index was greater than 150 during most of the radar soundings, sometimes picking 250

In 2003, there was a decrease and the F10.7 index values ranged between 100 and 150.

From 2006 up to 2010, the F10.7 index decreased below 100.

Methodology

- The magnetic field-aligned-integrated conductivity model -

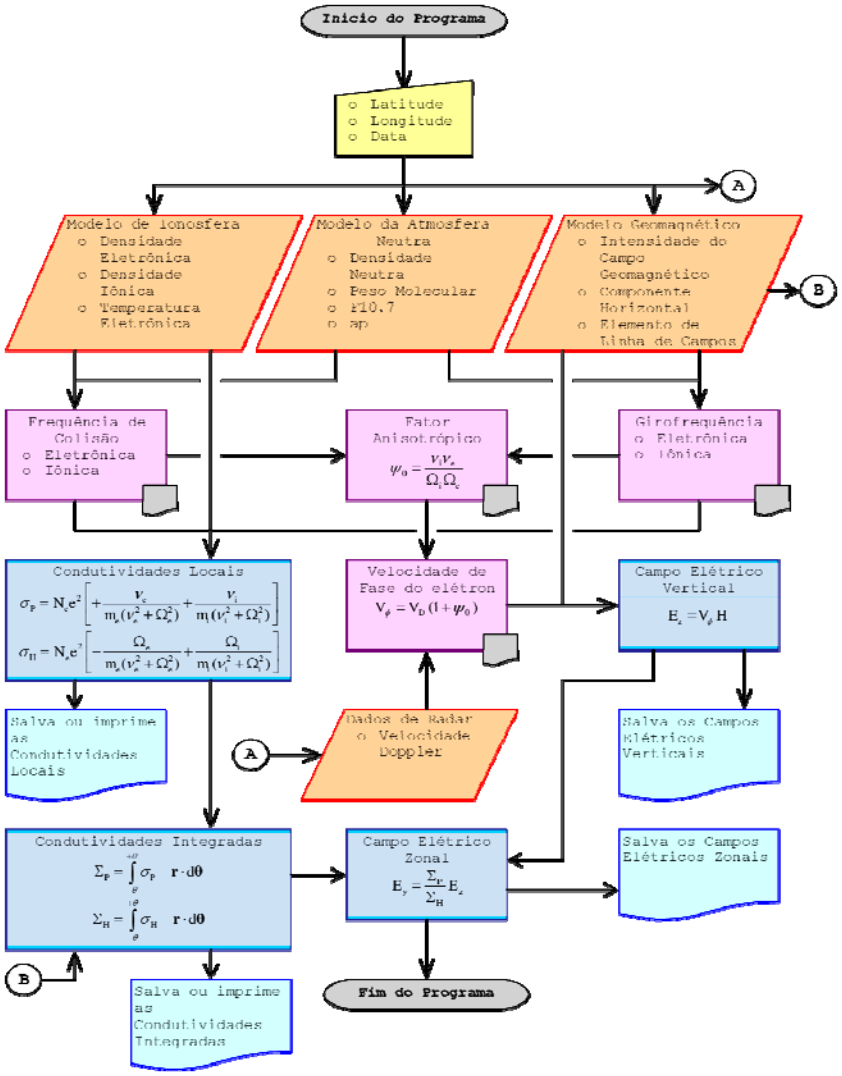

DEPENDENCES:

- It runs for American sector
- F10.7 Solar flux dependent
- ap index
- Collision frequencies by Schunk e Nagy (2000)
- IRI-2007, MSIS-2000, IGRF-11

ALGORITHM:

1) Anisotropic Factor
2) Doppler Velocity
3) Electron Velocity
4) Ez computations
5) Local conductivities estimate
6) Field-line integrated conductivities estimate
7) Ey computations

Methodology

- Model results examples -

CONDUTIVIDADE LOCAL HALL (S/m) – 07/02/2001 (a)

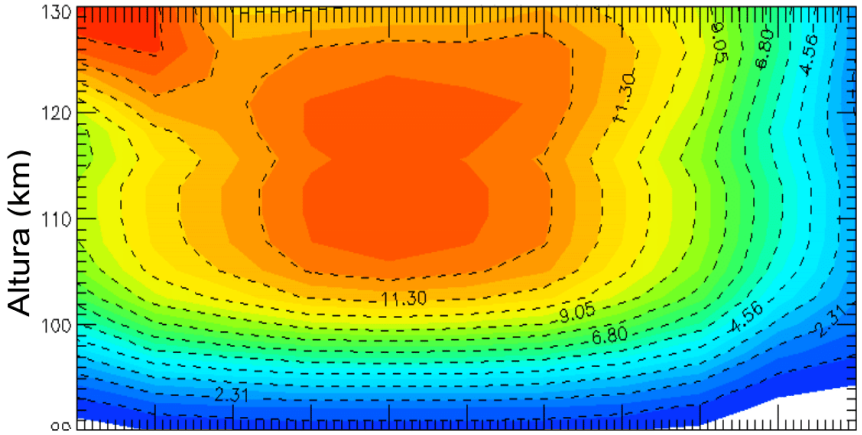

CONDUTIVIDADE LOCAL PEDERSEN (S/m) – 07/02/2001 (b)

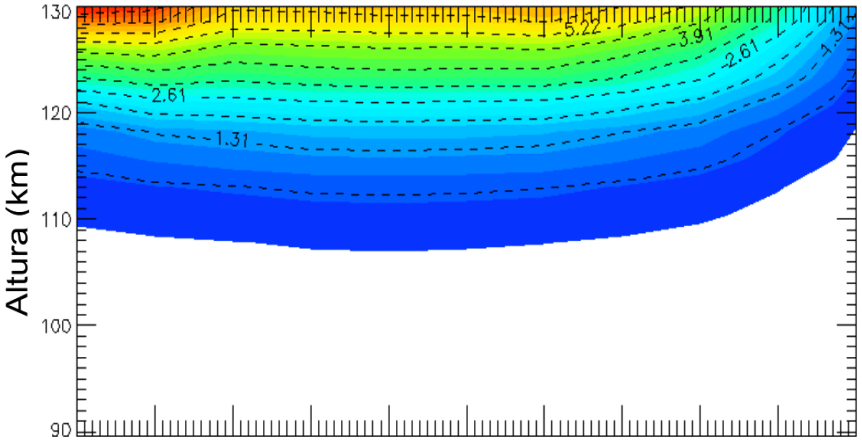

RAZÃO CONDUTIVIDADE HALL-PEDERSEN (S/m) – 07/02/2001 (c)

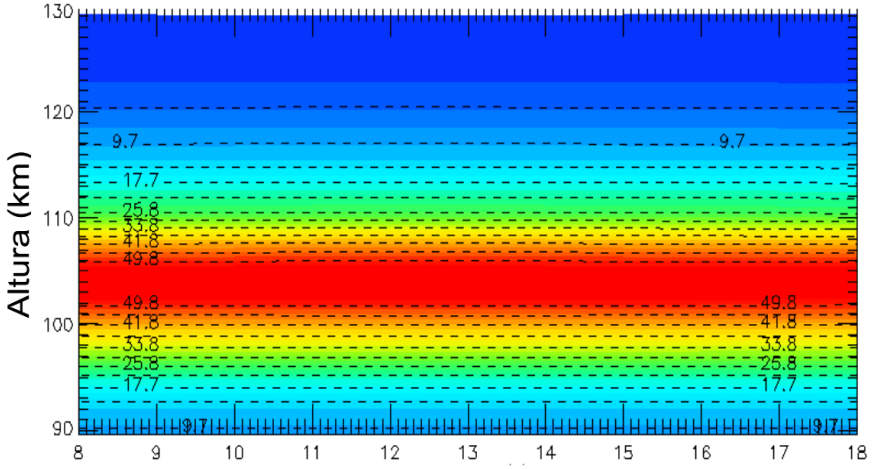

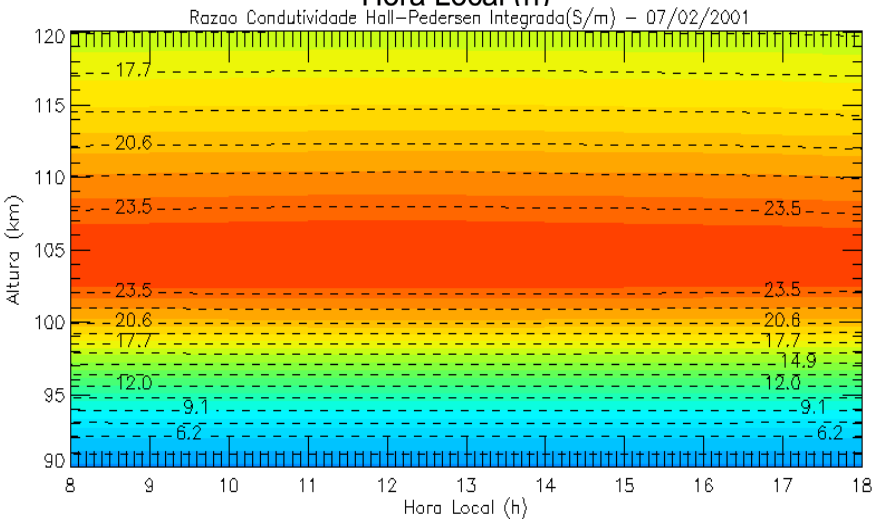

Methodology

- The influence of the different models in the electric field -

Table 1. Error estimating the Ey and Ez, with artificial 10%-error simultaneously introduced to the quantities provided from the MSIS-2000, IGRF-11 and IRI-2007 models for four range-heights.

Altura (km)	$\Delta Ey(\%)$		$\Delta Ez(\%)$	
	Dec. ($Ey_{0,9}$)	Acr. ($Ey_{1,1}$)	Dec. ($Ez_{0,9}$)	Acr. ($Ez_{1,1}$)
110,3	-4,79%	5,37%	-11,10%	11,48%
107,7	-8,71%	9,99%	-13,01%	14,05%
105,1	-15,72%	18,80%	-17,06%	19,49%
102,5	-22,00%	27,30%	-20,38%	23,96%
$\lvert Erro \rvert$	12,81%	15,37%	15,39%	17,25%

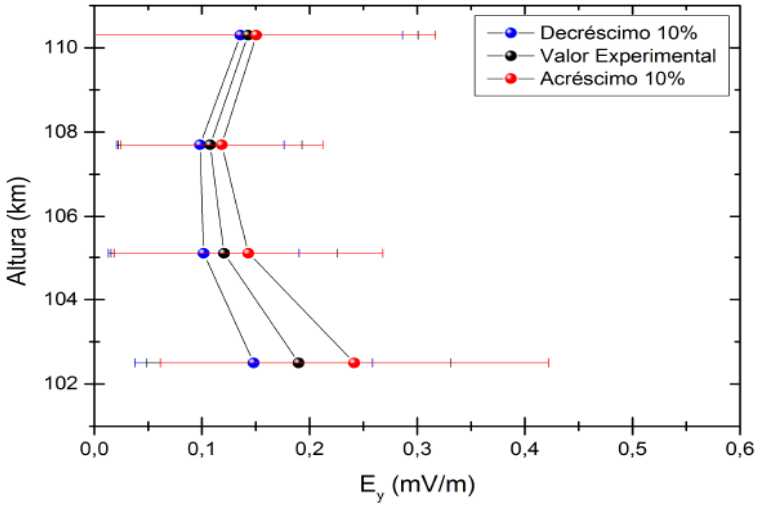

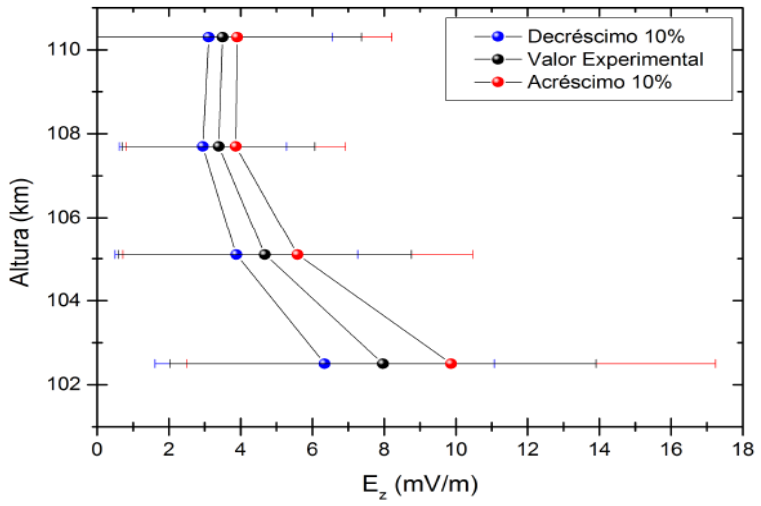

Results and Discussions

- The Ey and Ez diurnal variations -

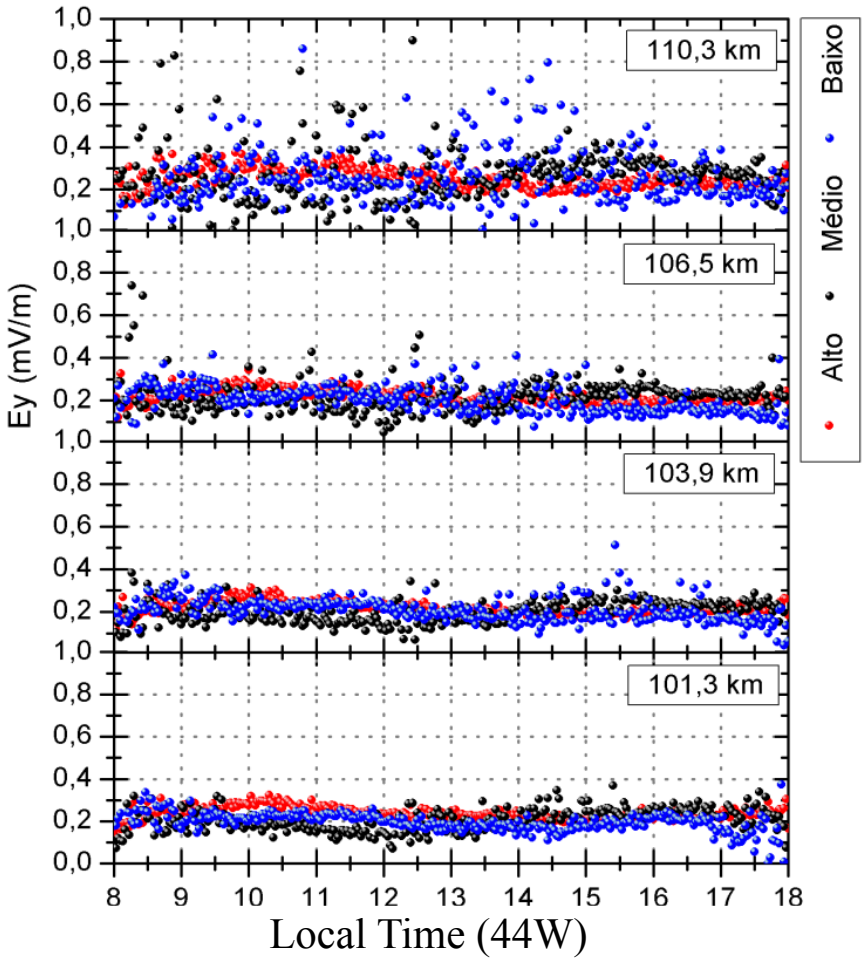

Ey

These graphs showed that Ey ranges from 0.19 to 0.35 mV/m between the 8 and 18 h (LT) in the Brazilian sector, and seems to have a small dependency with the solar activity.

We are not able to clearly identify the influence of the solar activity in its diurnal variation, independent of the height, except at 110.3 km at high solar activity when we have considerable data dispersions.

AFTER: Moro, J. (2015). Variações longitudinais dos campos elétricos do eletrojato equatorial no setor americano, Doutorado em Geofísica Espacial, Instituto Nacional de Pesquisas Espaciais, INPE, Brasil, p. 141. (sid.inpe.br/mtc-m21b/2015/01.28.15.49-TDI)

Results and Discussions

- The Ey and Ez diurnal variations -

Ez

It is notable that it is more intense during high solar flux, especially in the morning hours from 9 h and 13 h over all range-heights.

The Ez ranges from 4.65 to 10.12 mV/m and offers a more pronounced dependency is observed.

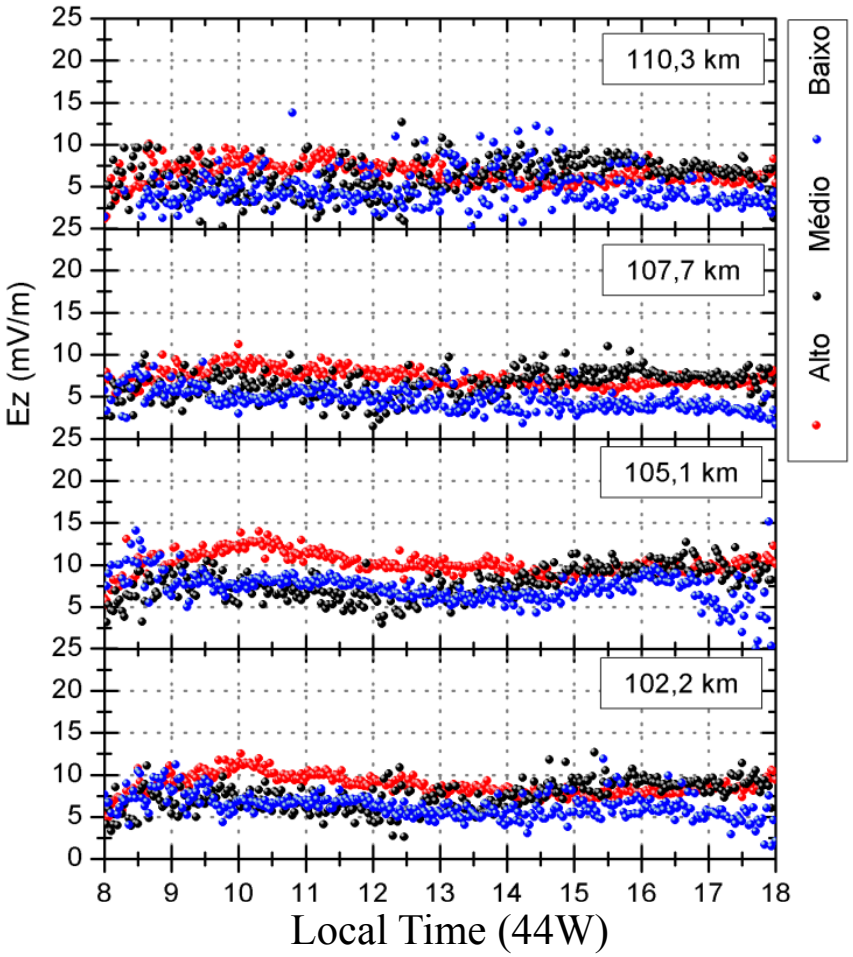

AFTER: Moro, J. (2015). Variações longitudinais dos campos elétricos do eletrojato equatorial no setor americano, Doutorado em Geofísica Espacial, Instituto Nacional de Pesquisas Espaciais, INPE, Brasil, p. 141. (sid.inpe.br/mtc-m21b/2015/01.28.15.49-TDI)

Results and Discussions

- The Ey and Ez average -

We observe:

- A positive gradient of Ey with height for low and average solar activity analyzing the daily average Ey, but not during high solar activity.
- A negative gradient of Ez irrespective the solar activity
- A proportional dependence of the Ez with the solar activity is clearly observed, in all the range heights.
- Ey increases at the lower portion of EEJ (below 105-107 km) and decreases in the upper portion (above 107 km) as the F10.7 increases,
- A tentative explanations: the solar flux F10.7 causes an increase ionization which leads to an increase of electron density causes an increase in Ey lower portion of EEJ, and reduces Ey at the top, as per our IRI-2007 analysis on the electric field computation

ht (km)	$\langle Ey \rangle \pm \langle Erro \rangle$	$\langle Ez \rangle \pm \langle Erro \rangle$
10,3	0,25 ± 0,04	6,58 ± 1,23
07,7	0,22 ± 0,03	7,29 ± 0,94
05,1	0,21 ± 0,02	8,76 ± 1,20
02,5	0,23 ± 0,03	10,12 ± 1,30
10,3	0,27 ± 0,12	6,29 ± 2,04
07,7	0,22 ± 0,07	6,50 ± 1,60
05,1	0,20 ± 0,05	7,47 ± 1,72
02,5	0,20 ± 0,05	7,81 ± 1,87
10,3	0,26 ± 0,12	4,70 ± 2,13
07,7	0,20 ± 0,06	4,65 ± 1,26
05,1	0,20 ± 0,05	6,28 ± 1,46
02,5	0,19 ±0,04	7,24 ± 1,82

ricos do eletrojato equatorial no setor americano, Doutorado em Geofísica Espacial, Instituto Nacional de Pesquisas Espaciais, INPE, Brasil, p. 141. (sid.inpe.br/mtc-m21b/2015/01.28.15.49-TDI)

Summary

- We were not able to clearly identify the influence of the solar activity in its diurnal variation of the Ey, while Ez is notable more intense during high solar flux, especially in the morning hours from 9 h and 13 h over all range-heights.
- We observe a positive gradient of Ey with height for low and average solar activity analyzing the daily average Ey, but not during high solar activity. The gradient of Ez remained negative irrespective the solar activity and a proportional dependence of the Ez with the solar activity is clearly observed, in all the range heights.
- We also identify that the Ey increases at the lower portion of EEJ (below 105-107 km) and decreases in the upper portion (above 107 km) as the F10.7 increases, and a tentative explanations was presented in terms of the increase in the solar flux F10.7 causes an increase ionization which leads to an increase of electron density causes an increase in Ey lower portion of EEJ, and reduces Ey at the top, as per our IRI-2007 analysis on the electric field computation.
- In conclusion, the zonal electric field, which normally ranged from 0.19 to 0.35 mV/m between the 8 and 18 h (LT) in the Brazilian sector, presented a small dependency with the solar activity. The vertical electric field, which normally ranges from 4.65 to 10.12 mV/m, presented a more pronounced dependency, although. But, we see no appreciable dependence in the amplitude of the electrical field at the E region range-heights investigated.

Acknowledgement

CNPq
Conselho Nacional de Desenvolvimento Científico e Tecnológico

FAPESP

Scholarship in Research Productivity
(Grants 305242/2011-3)
Research Thematic Project
(Grants 2012/08445-9)

Contact Information

Clezio M. De Nardin - clezio.denardin@dae.inpe.br
http://www.dae.inpe.br/~clezio.denardin/

Instituto Nacional de Pesquisas Espaciais
C. P. 515
CEP 12201-970
São José dos Campos. SP - Brazil

+55 12 3208 7180 (Secretary)
+55 12 3208 7055 (Direct)

+55 12 3208 6990

PROGRAM FOR

ESTUDO E MONITORAMENTO BRASILEIRO DO CLIMA ESPACIAL

www.inpe.br/climaespacial